Yang W, Peng Z, Wei K, Shi P, Tian W.

Superiorities of Variational Mode Decomposition over Empirical Mode Decomposition Particularly in Time-frequency Feature Extraction and Wind Turbine Condition Monitoring.

***IET Renewable Power Generation* (2016)**

DOI: 10.1049/iet-rpg.2016.0088

Superiorities of Variational Mode Decomposition over Empirical Mode Decomposition Particularly in Time-frequency Feature Extraction and Wind Turbine Condition Monitoring

Wenxian Yang [1,2*], Zhike Peng [3], Kexiang Wei [1], Pu Shi [2], Wenye Tian [2]

[1] Hunan Province Cooperative Innovation Centre for Wind Power Equipment and Energy Conversion, Hunan Institute of Engineering, Xiangtan 411101, China

[2] School of Marine Science and Technology, Newcastle University, Newcastle upon Tyne NE1 7RU, UK

[3] State Key Laboratory of Mechanical System and Vibration, Shanghai Jiaotong University, Shanghai 200240, China

* Wenxian.yang@ncl.ac.uk

Abstract

Due to constantly varying wind speed, wind turbine (WT) rotor and the other drive train components often operate at variable speeds in order to capture energy from wind as efficiently as possible and therefore generate more electric power. Due to the variable loads and rotational speed, the condition monitoring (CM) signals collected from WTs always contain intra-wave features, which are difficult to extract through performing conventional Time-Frequency Analysis (TFA) because the successful extraction of these intra-wave characteristics requests a locally adaptive signal processing technique. To now, only Empirical Mode Decomposition (EMD) and its extension form can meet such a requirement. However, practice has shown that the EMD and those EMD-based techniques also suffer a number of defects in TFA (e.g. weak robustness of against noise, unidentified ripples, inefficiency in detecting side-band frequencies, etc.). The existence of these issues has significantly limited the extensive application of the EMD family techniques to WT CM. Recently, an alternative TFA method, namely Variational Mode Decomposition (VMD), was proposed to overcome all these issues. The purpose of this paper is to verify the superiorities of the VMD over the EMD and investigate its potential application to the future WT CM. Experiment has shown that the VMD outperforms the EMD not only in noise robustness but also in multi-component signal decomposition, side-band detection, and intra-wave feature extraction. Thus, it has potential as a promising technique for WT CM.

Keywords: wind turbine, condition monitoring, variational mode decomposition, empirical mode decomposition

1. Background

Wind turbine (WT) condition monitoring (CM) has been widely accepted as one of the most effective approaches to reducing the Cost of Energy (COE) of wind power [1-7], premised on that CM is able to give reliable indication and prediction to the actual health condition of the WTs and their components. While, reliable CM relies on the use of effective signal processing tools, which enable the successful extraction of those fault-related features from WT CM signals.

Nowadays, variable speed control is adopted by most large mega-watt scale WTs to adapt for constantly varying wind load and enable WTs to work efficiently over a wide range of wind speeds. Such a control strategy does maximize WT power generation. However, it also brings challenge to WT CM at the same time because intra-wave features are present in the WT CM signals when the WT rotates at variable speeds. The successful extraction of these intra-wave features requests locally adaptive signal processing technique that can match the gradual evolution of the time waveform of the signal. However, so far most Time-Frequency Analysis (TFA) tools, except the Empirical Mode Decomposition (EMD) [8] and its extension forms (e.g. Local Mode Decomposition (LMD) [9] and Intrinsic Time-scale Decomposition (ITD) [10]), are not locally adaptive in nature.

In contrast to conventional TFA methods, the EMD and LMD provide more realistic signal representations without artifacts imposed by the non-adaptive limitations of both Fourier- and Wavelet-transform based TFA methods. They are completely adaptive to the change of signal waveforms and decompose the signal into a limited number of Intrinsic Mode Functions (IMFs) or production functions through automatically performing a series of recursive calculations. These decomposed functions represent the fundamental oscillatory modes of the signal, from which the instantaneous time-frequency features of interest are deemed to be observed. This enables the EMD-based methods have potential as promising tools for dealing with the engineering problems associated with the analysis of intra-wave signals, for example sea waves, earthquake waves, biomedical signals and so on. In recent years, the application of EMD and its extension forms (such as LMD and ITD) have been extended to the field of machine CM [8-19]. However, practice

has disclosed that the EMD and its extension forms also show the following defects in signal processing and feature extraction:

- **weak robustness of against noise**. The EMD-based techniques are sensitive to the noise contained in the signal. A little change in the Signal-to-Noise Ratio (SNR) of the signal can lead to significantly different signal decomposition results. Such a phenomenon inspired the development of Ensemble Empirical Mode Decomposition (EEMD) [20];
- **unidentified features**. Unidentified 'ripples' are often present in the results obtained from EMD-based techniques, particularly at low frequencies [8]. They spoil the time-frequency features of the signal and thus increase the difficulty of signal interpretation;
- **inefficient capability in decoupling frequency components**. The EMD-based techniques have limitations in distinguishing different components in narrowband signals [21]. They often allocate those frequency components in immediate vicinity into the same decompose function by mistake. As a consequence, the fault-related instantaneous time-frequency features, such as the side-band characteristics induced by fault, cannot be successfully extracted from the signal.

All these disadvantages discount the added value of the EMD-based techniques in signal processing and thus significantly limit their extensive application to machine CM, despite the lots of efforts for improvement, such as the work reported in [9], [20], [22] and so on. To address these issues, an alternative signal processing tool, namely Variational Mode Decomposition (VMD), was developed recently [23]. It has been claimed that in theory, the VMD outperforms the EMD in tone detection, tone separation, and noise robustness [23]. These merits potentially enable the VMD to be an effective tool for processing non-stationary signals and implementing machine CM tasks. In order to investigate the actual benefit of the VMD in real life, the comparison of the VMD and the EMD were performed quite recently in a few literatures [24-27]. However, the comparisons performed in the reported literatures lack depth, i.e. they mainly focus on comparing the time-waveforms of the functions decomposed respectively by the VMD and EMD, rather than investigating their different capabilities in tone detection, tone separation and noise robustness as well as the superiorities of the VMD in extracting instantaneous time-frequency features from non-stationary signals. For this reason, a depth investigation of the non-stationary signal processing capability of the VMD is further conducted in this paper via both numerical simulation and experimental approaches. Its superiorities in tone detection, tone separation, noise robustness and

instantaneous time-frequency feature extraction are demonstrated through the comparison with the EMD.

The remaining part of the paper is arranged as follows. Firstly, the fundamental theory of the VMD is explained in Section 2; secondly, the superiorities of the VMD over the EMD in tone detection, tone separation, noise robustness and time-frequency feature extraction are experimentally verified in Section 3; thirdly, the potential application of the VMD to WT CM is investigated in Section 4. The paper is finally concluded in Section 5.

2. Variational mode decomposition (VMD)

According to [23], the VMD decomposes an original signal $f(t)$ into a given number of modes $(u_k(t), k = 1,2,3, \dots \dots, K)$ either exactly or in a least squares sense, i.e.

$$f(t) = \sum_{k=1}^{K} u_k(t) \tag{1}$$

where the number of modes K is defined in advance. $u_k(t)$ are narrow-band mode functions. They can be written as

$$u_k(t) = A_k(t)\cos(\phi_k(t)) \tag{2}$$

where $A_k(t)$ and the time derivative of phase change $\phi_k'(t)$ are assumed to be positive and slowly varying component compared to phase $\phi_k(t)$.

The decomposed modes have specific sparsity property while reproducing the input signal. In other words, each mode is mostly compact around a central frequency. To reach this purpose, the bandwidth of every mode is assessed by using the following scheme:

Step 1: For each mode $u_k(t)$, compute the associated analytic signal $\mathcal{H}\left(u_k(t)\right)$ by means of the Hilbert transform, i.e.

$$\mathcal{H}u_k(t) = \frac{1}{\pi} p.v. \int_{\mathbb{R}} \frac{u_k(v)}{t-v} dv \tag{3}$$

Then, a new analytic function $u_k(t) + j\mathcal{H}u_k(t)$ $(j = \sqrt{-1})$ can be formed, which is a unilateral frequency spectrum.

Step 2: Shift the frequency spectrum of the mode to "baseband" by mixing with an exponential function tuned to the estimated central frequency ω_k of the mode.

$$u_k^M = \left(u_k(t) + j\mathcal{H}u_k(t)\right)e^{-j\omega_k t} \tag{4}$$

Step 3: Then, the bandwidth of the inspected mode can be estimated through the *H1* Gaussian smoothness of the demodulated signal, i.e. the squared *L*2 norm of the gradient,

$$BW_k = \left\| \partial_t \left[\left(\left(\delta(t) + \frac{j}{\pi t} \right) * u_k(t) \right) e^{-j\omega_k t} \right] \right\|_2^2 \tag{5}$$

This is associated with a constrained variational problem, i.e.

$$\min_{u_k, \omega_k} \left\{ \sum_k \left\| \partial_t \left[\left(\left(\delta(t) + \frac{j}{\pi t} \right) * u_k(t) \right) e^{-j\omega_k t} \right] \right\|_2^2 \right\} \quad s.t. \ \sum_k u_k = f \tag{6}$$

In order to render the problem unconstrained, both a quadratic penalty term and Lagrangian multipliers are used to construct the following augmented Lagrangian:

$$\mathcal{L}(u_k, \omega_k, \lambda) = \alpha \sum_k \left\| \partial_t \left[\left(\left(\delta(t) + \frac{j}{\pi t} \right) * u_k(t) \right) e^{-j\omega_k t} \right] \right\|_2^2 + \|f - \sum_k u_k\|_2^2 + \langle \lambda, f - \sum_k u_k \rangle \tag{7}$$

where, α is a parameter designed to control the bandwidth of the filter.

The resultant constrained variational problem can be solved by separating minimizations with respect to the resultant modes $\{u_k\}$ and their corresponding central frequencies $\{\omega_k\}$.

Based on the theory depicted above, the VMD is implemented via the following computing algorithm:

(1) Define the number of modes K;

(2) Initialize $\{\hat{u}_k^1\}$, $\{\omega_k^1\}$, $\hat{\lambda}^1$, and $n = 0$;

(3) Update n with $n + 1$, and repeat the following loop

For $k = 1{:}K$

Update $\hat{u}_k$ *for all* $\omega \geq 0$ *with*

$$\hat{u}_k^{n+1}(\omega) = \frac{\hat{f}(\omega) - \sum_{i<k} \hat{u}_i^{n+1}(\omega) - \sum_{i>k} \hat{u}_i^n(\omega) + \frac{\hat{\lambda}^n(\omega)}{2}}{1 + 2\alpha(\omega - \omega_k^n)^2} \tag{8}$$

Update ω_k *with*

$$\omega_k^{n+1} = \frac{\int_0^\infty \omega |\hat{u}_k^{n+1}(\omega)|^2 d\omega}{\int_0^\infty |\hat{u}_k^{n+1}(\omega)|^2 d\omega} \tag{9}$$

End for.

Dural ascent for all $\omega \geq 0$

$$\hat{\lambda}^{n+1}(\omega) = \hat{\lambda}^{n}(\omega) + \tau\left(\hat{f}(\omega) - \sum_k \hat{u}_k^{n+1}(\omega)\right) \tag{10}$$

Until the following convergence condition is satisfied

$$\sum_{k=1}^{K} \frac{\left\|\hat{u}_k^{n+1} - \hat{u}_k^{n}\right\|_2^2}{\left\|\hat{u}_k^{n}\right\|_2^2} < \varepsilon \tag{11}$$

where, $\hat{f}$ represents the Fourier transform of original signal $f(t)$.

From the algorithm depicted above, there are two key parameters that can affect the VMD results. They are

- the number of modes K; and
- bandwidth control parameter α

The former is determined based on the number of frequency components included in the signal being inspected, while the latter is determined based on the central frequency of interest. They are correlated to each other. In theory,

- a large number of modes would lead to redundant VMD information, while a small number of modes would result in the phenomenon of mode mixing in the VMD results;
- the smaller the value of bandwidth control parameter, the wider the bandwidth of the filter tends to be. When the bandwidth of the filter is wide, more background noise and interference items will be included in the VMD result. But if the filter bandwidth is too narrow, the VMD results are likely to be distorted sometimes.

From these reasons, both parameters K and α should be optimised to assure the accuracy of the VMD. Since this paper is focused only on investigating the superiorities of the VMD in contrast to the EMD rather than improving the VMD, the achievements on optimized VMD will be reported in a separate paper.

3. Verification of the VMD

In this section, the superiorities of the VMD over the EMD in noise robustness, multi-component signal decomposition, side-band feature detection, and intra-wave signal interpretation will be investigated. Herein, it is necessary to repeat once again that the number of modes K used for VMD calculation needs to be defined in advance. However, how to define an appropriate value of K is still an open question remaining to resolve. In this paper, to facilitate the comparison of the

VMD and EMD the number of IMFs resulted by the EMD in corresponding scenario will be taken as the value of K.

3.1 Noise robustness

To investigate the noise robustness performance of the VMD, a simulated signal $x(t)$ is designed, which is the sum of a harmonic signal and white noise $\sigma(t)$.

$$x(t) = \sin(2\pi f t) + \sigma(t) \tag{12}$$

where $f = 70\text{Hz}$, $t = 0\sim1\text{s}$.

When the Signal-to-Noise Ratio (SNR) is 10 dB, the time waveform of the discrete signal collected by using a sampling frequency of 1000 Hz is shown in Fig.1, from which it can be clearly seen that the harmonic signal has been seriously distorted by noise. Then, both the VMD and EMD are applied to processing the signal and the corresponding results are shown in Fig.2.

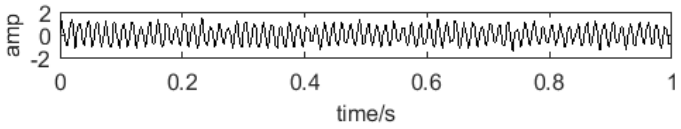

Fig.1 Noise polluted signal

The comparison of Figs.2a and 2b shows that the VMD shows more powerful capability than the EMD in filtering white noise from $x(t)$, i.e. the white noise distributed in different frequency bands has been successfully extracted out by the VMD, see modes 1, 2, 4, 5 and 6 shown in Fig.2a. By contrast, the noise, particularly those in high-frequency bands, are not successfully extracted out by the EMD, see the IMFs shown in Fig.2b. This implies that noise still exists in the resultant IMFs by the EMD. As a consequence, the 70 Hz harmonic component is seriously smeared in the time-frequency map shown in Fig.2d, while it has been precisely illustrated in Fig.2c. From this example, it is sure that the VMD does surpass the EMD on noise robustness. Herein, it is worthy to note that the time-frequency maps shown in Figs.2c and 2d are obtained by simply performing the Hilbert transforms of the 'modes' and 'imfs' respectively in Figs.2a and 2b. This is a standard method adopted by the Hilbert-Huang transform to extract the instantaneous time-frequency features from nonlinear, non-stationary signals [21].

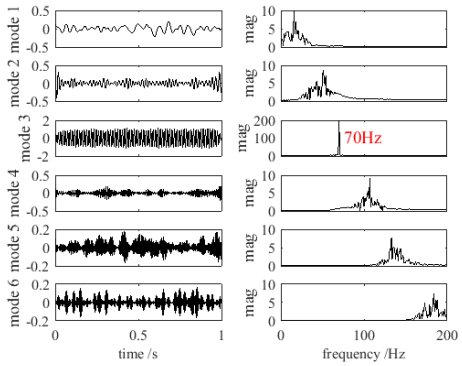

(a) Modes by the VMD

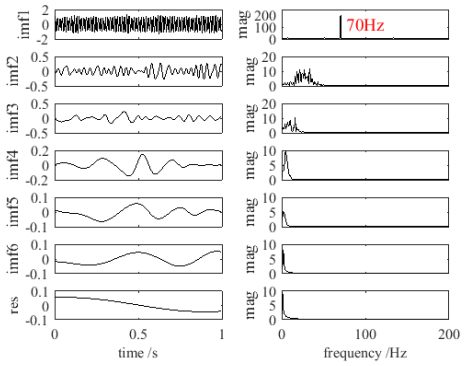

(b) IMFs by the EMD

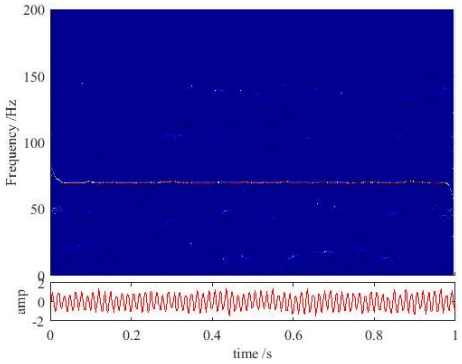

(c) Time-frequency map by the VMD

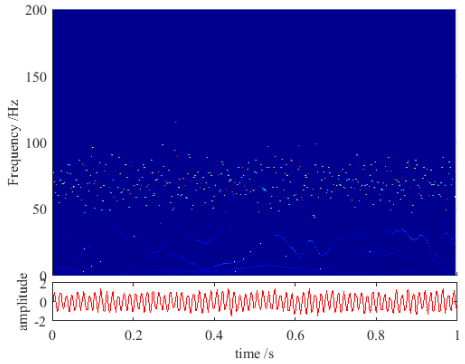

(d) Time-frequency map by the EMD

Fig.2 Verification of noise robustness

3.2 Multi-component signal decomposition

Assume a multi-component signal $x(t)$

$$x(t) = \sin(2\pi f_1 t) + \sin(2\pi f_2 t) + \sin(2\pi f_3 t) \tag{13}$$

consisting of three harmonic components. $f_1 = 30\text{Hz}$, $f_2 = 50\text{Hz}$, and $f_3 = 70\text{Hz}$. Apply both the VMD and EMD to decomposing the signal and the corresponding results are shown in Fig.3.

From Fig.3, it is found that the VMD has successfully decoupled the three harmonic components 30Hz, 50Hz and 70Hz in the raw signal and moreover allocated them correctly to right modes. By contrast, the EMD fails to correctly decouple these three frequency components. The components of 50Hz and 70Hz are wrongly allocated to the same IMF function. The 30Hz component is allocated into IMF2, but a small leakage of it still can be observed from IMF1. Due to this unsatisfactory signal decomposition result by the EMD, the three frequency components are smeared in the time-frequency map shown in Fig.3d. In comparison, the three frequency components are explicitly illustrated in the time-frequency map in Fig.3c despite the distortions

appearing at both sides of boundaries. Thus, it can be said that the VMD does outperform the EMD in multi-component signal decomposition. Moreover, such a powerful tone separation capability of the VMD is also extended to detecting side-band features, which are often related to the presence of a fault.

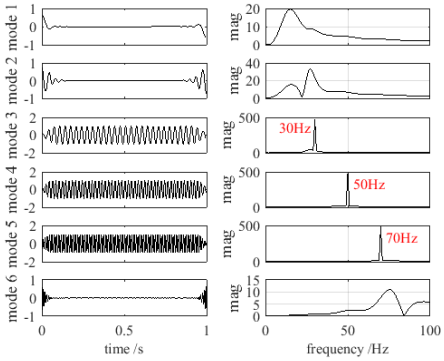

(a) Modes by the VMD

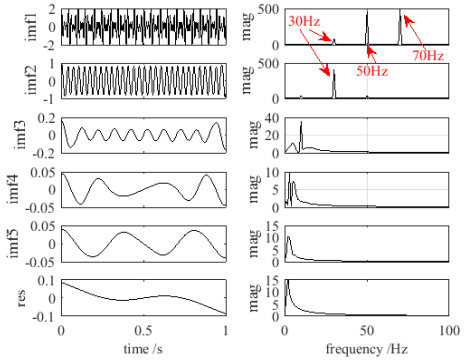

(b) IMFs by the EMD

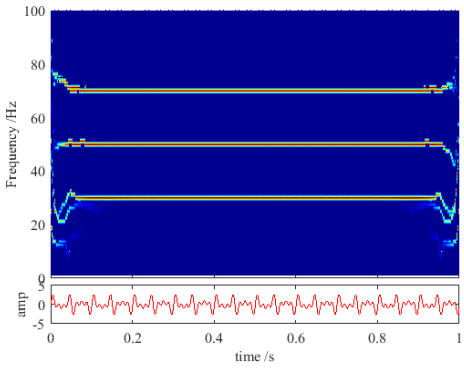

(c) Time-frequency map by the VMD

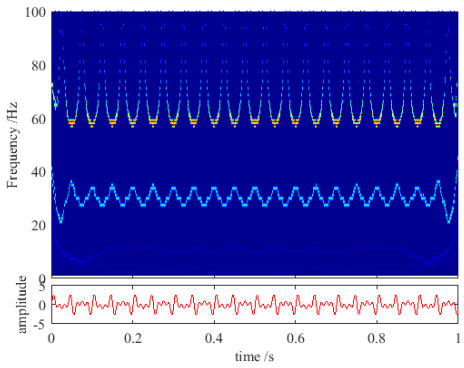

(d) Time-frequency map by the EMD

Fig.3 Verification of multi-component signal decomposition

3.3 Side-band feature detection

In order to demonstrate the capability of the VMD in detecting side-band features, the following signal is simulated and its corresponding VMD and EMD results are shown in Fig.4.

$$x(t) = 0.2\sin(2\pi f_1 t) + \sin(2\pi f_2 t) + 0.2\sin(2\pi f_3 t) \qquad (14)$$

where $f_1 = 45\,\mathrm{Hz}$, $f_2 = 50\,\mathrm{Hz}$, and $f_3 = 55\,\mathrm{Hz}$. The first and third items in the equation are designed with small amplitude in order to simulate weak side-band frequency components induced by fault.

From Fig.4a, it is found that although the three frequencies are very close to each other and the side-band components are insignificant in amplitude, both side-band components have been successfully detected by the VMD and perfectly decoupled from the central frequency 50Hz. Thanks to this successful decomposition, all three frequency components are correctly illustrated in the time-frequency map shown in Fig.4c. On the contrary, the EMD fails to perform successful detection of the side-band features. All three frequency components are wrongly allocated into the same IMF. As a consequence, only the central frequency 50Hz can be identified from the time-frequency map in Fig.4d. The map does not give any indication to both side-band frequencies. Through this experiment, it can be said that the EMD is inefficient in side-band feature detection, while the VMD shows a powerful capability in this aspect.

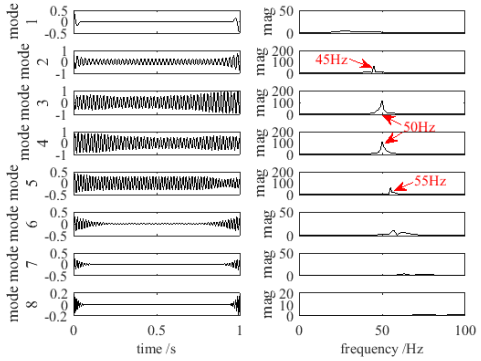

(a) Modes by the VMD

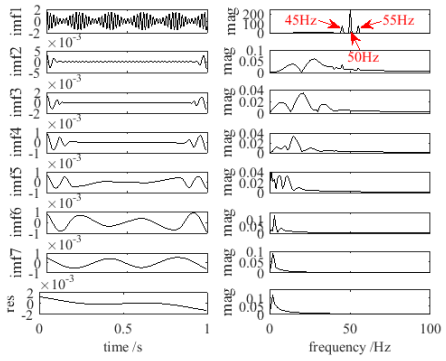

(b) IMFs by the EMD

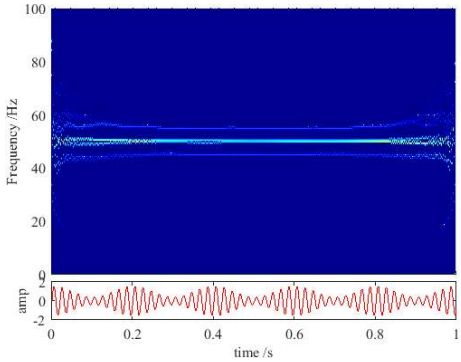

(c) Time-frequency map by the VMD

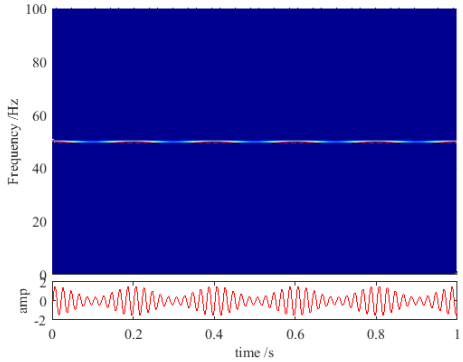

(d) Time-frequency map by the EMD

Fig.4 Verification of side-band feature extraction

3.4 Intra-wave signal interpretation

From the computing algorithm described in Section 2, it can be inferred that the VMD is, in essence, a signal filtering technique originated from the Hilbert transform. It is not locally adaptive.

Thus, it is essential to verify its capability in processing intra-wave signals. In addition, considering the VMD will be applied to interpreting WT gearbox signals that are often modulated by a number of exciting sources, the following signal is deliberately designed to test the capabilities of the VMD in interpreting intra-wave and amplitude-modulated signals.

$$x(t) = \begin{cases} \sin(2\pi f_1 t) & 0 \le t < 0.5s \\ \sin\left(2\pi f_{chirp} t\right) & 0.5s \le t < 1s \\ \sin(2\pi f_2 t)\sin(2\pi f_3 t) & 1s \le t \le 1.5s \end{cases} \quad (15)$$

where $f_1 = 10\text{Hz}$, $f_2 = 100\text{Hz}$, $f_3 = 5\text{Hz}$, and the chirp frequency f_{chirp} increases linearly from f_1 to f_2 over the time from 0.5s to 1s.

To ease understanding, the time waveform of the signal is shown in Fig.5. Likewise, both the VMD and EMD are applied to the signal and the corresponding results are shown in Fig.6.

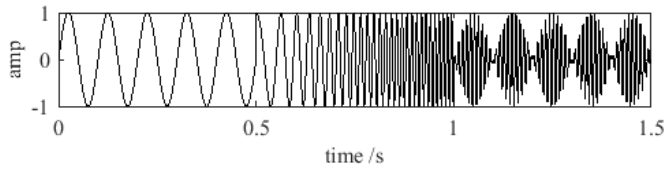

Fig.5 Intra-wave signals

From Fig.6, it is found that the intra-wave feature has been successfully extracted out by both the VMD and the EMD. However, the comparison suggests that the VMD is still superior to the EMD because the EMD generates unidentified components while the VMD does not. These unidentified frequency components spoil the time-frequency map and consequently make signal interpretation more difficult. In addition, from Fig.6 it is seen that the amplitude modulation feature $|f_1 \pm f_2|$ have been successfully detected also by the VMD, from which frequencies f_1 and f_2 can be readily derived. By contract, the modulation feature cannot be observed at all from the EMD results.

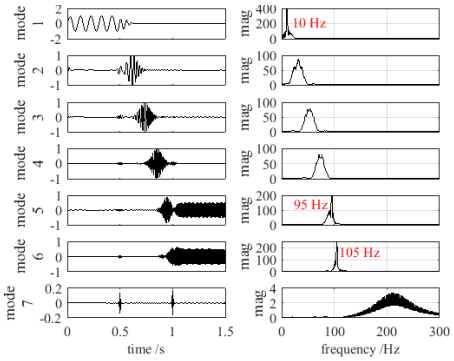

(a) Modes by the VMD

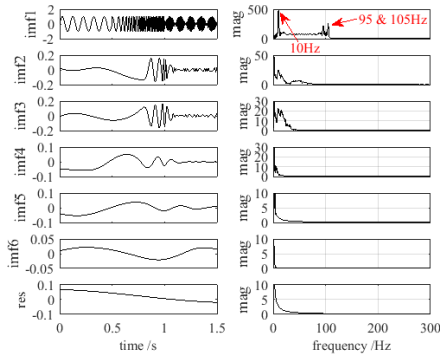

(b) IMFs by the EMD

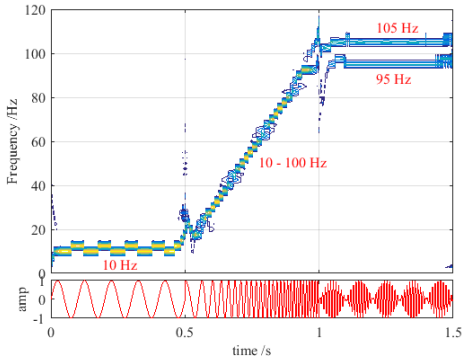

(c) Time-frequency map by the VMD

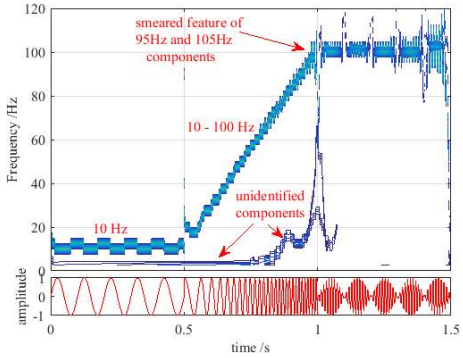

(d) Time-frequency map by the EMD

Fig.6 Intra-wave feature extraction and signal modulation detection

From the above experiments, it can be concluded that the VMD does outperform the EMD on the performance of noise robustness, tone detection, tone separation and time-frequency feature extraction. All these superiorities enable the VMD to have potential as a promising tool for WT CM. Accordingly, experiments are further conducted on test rig in the next section in order to verify this potential capability of the VMD.

4. Applications to WT CM

To investigate the potential of the VMD in WT CM, in this section the VMD is applied to detect both a mechanical and an electrical fault occurring in 'geared WTs'. The vibration signal used for detecting the mechanical fault was collected from the high-speed stage of the gearbox in an operating WT, while the electric power signal used for detecting the electrical fault was collected from the induction generator in a WT CM test rig.

4.1 Mechanical fault detection

The raw gearbox vibration signal was collected by using a sampling frequency of 20 kHz. Its time waveform is shown in Fig.7, where the vibration acceleration data collected before and after the gear tooth surface was damaged (i.e. pitted) are integrated into one signal for facilitating the understanding of fault detection results.

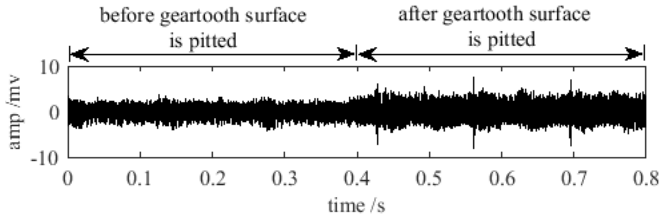

Fig.7 Raw gearbox vibration signal

In order to highlight the powerful feature extraction ability of the VMD in WT CM, in the experiment both the VMD and EMD are applied to interpret the vibration signal shown in Fig.7. The corresponding signal analysis results are shown in Fig.8.

From Fig.8, it is found that in comparison of the EMD, the VMD accomplishes a precise decomposition of the signal, i.e. the raw vibration signal is manifested by 14 modes that are sorted in ascending frequency order. These modes are ‘not exactly’ but are nearly mono-component signals attributed to their limited bandwidth, see Fig.8a. In contrast to the VMD, the EMD decomposes the signal into 13 IMFs and 1 residual component. The IMFs are sorted in descending frequency order. But their frequency bandwidth is not constrained at all. For example, from Fig.8b it is clearly seen that both IMF1 and IMF2 have very wide bandwidth. It is such a defect leads to the smeared time-frequency features in Fig.8d. This is because the instantaneous time-frequency features of the signal always cannot be extracted satisfactorily by the means of the Hilbert transform if the signal being investigated has wide bandwidth. Such a point of view is also supported by the signal decomposition and feature extraction results shown in Figs.3, 4 and 6. On the contrary, the Hilbert transform can work very well in extracting the instantaneous time-frequency features if the signal of interest has limited bandwidth. Also for this reason, the time-frequency features that indicate the pitted gear tooth surface are precisely illustrated in Fig.8c. It has no doubt that the VMD has shown success in detecting this gear tooth fault, while the EMD fails in fault detection.

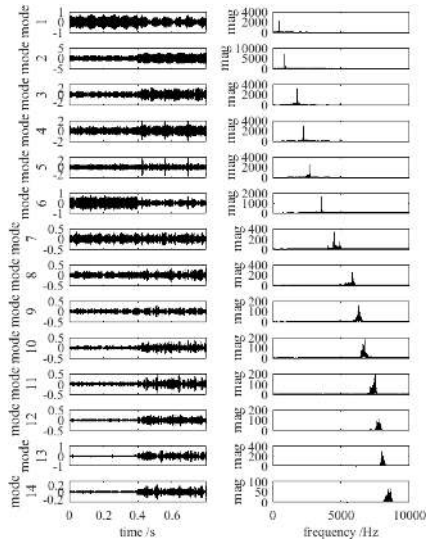

(a) Modes by the VMD

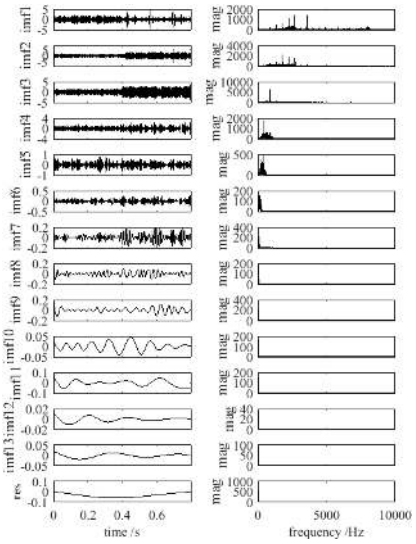

(b) IMFs by the EMD

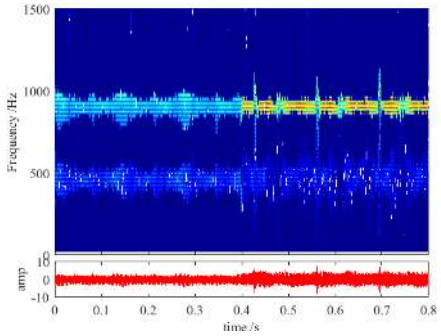

(c) Time-frequency map by the VMD

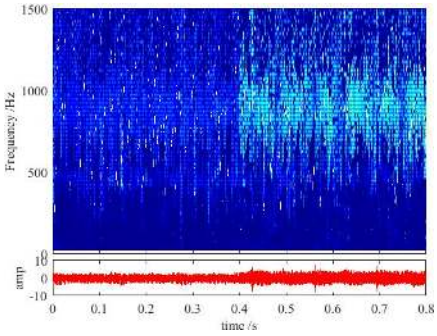

(d) Time-frequency map by the EMD

Fig.8 Detection of the fault occurring in the gearbox of an operating WT

4.2 Electrical fault detection

As mentioned above, the signal used in this section was collected from the generator of a geared WT CM test rig by using a sampling frequency of 5 kHz. The test rig comprises a 54 kW dc variable-speed motor, a two-stage gearbox and a 30 kW two pole pair induction generator, instrumented and controlled using LabVIEW [28]. To simulate the variable operational conditions of an operating WT, a variety of wind speed inputs were applied to the test rig via the dc motor, the speed of which was controlled by an external model incorporating the properties of natural wind at a variety of speeds and turbulences. In the experiment, the generator rotor was connected to an external load bank, allowing the simulation of generator electrical asymmetry faults via adjusting the phase resistances in the load bank. When the rotor phase resistances are repeatedly adjusted to be imbalanced, the electric power signal collected from the variable speed generator is

shown in Fig.9. Since for a two pole pair induction generator, the generator electrical signals will be modulated twice by the slip frequency as the rotor asymmetry moves through the air gap magnetic field twice for every pole pair cycle, the twice slip frequency can be regarded as the characteristic frequency for detecting the generator electrical asymmetry fault. Therefore, to ease fault detection the corresponding twice slip frequency against the variable rotational speed of the generator is also calculated and shown in Fig.9.

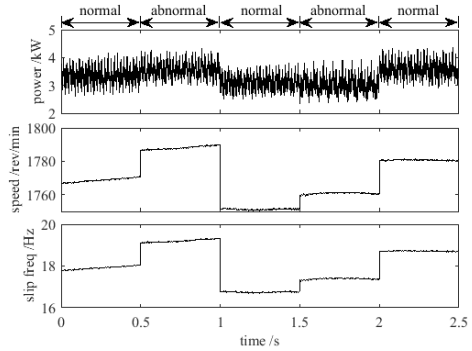

Fig.9 Generator electrical signal from a WT CM test rig

Likewise, both the VMD and EMD were applied to interpret the electric power signal in Fig.9 and the corresponding signal processing results are shown in Fig.10.

From Fig.10, it is found that all merits of the VMD in contrast to the EMD in signal decomposition and feature extraction have been demonstrated once again, i.e. the raw signal is precisely decomposed into a number of modes with limited frequency bandwidth, which allows a correct description of the instantaneous time-frequency features in Fig.10c by the means of the Hilbert transform. From Fig.10c, it is seen that despite the variable rotational speed, the fault-related twice slip frequency component is present immediately as soon as the generator rotor becomes asymmetry, while it is absent when the rotor phases are electrically symmetry. Undoubtedly, the generator electrical asymmetry fault can be readily detected from this observation. In comparison, Fig.10b shows that the EMD resultant IMFs are not necessary limited bandwidth signals. Their instantaneous time-frequency features cannot be correctly detected by using the Hilbert transform. As a consequence, they smear the time-frequency features in Fig.10d, increase the difficulty of CM, and make it impossible to implement fault detection.

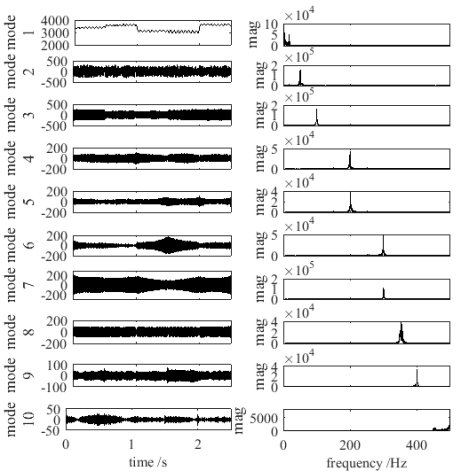

(a) Modes by the VMD

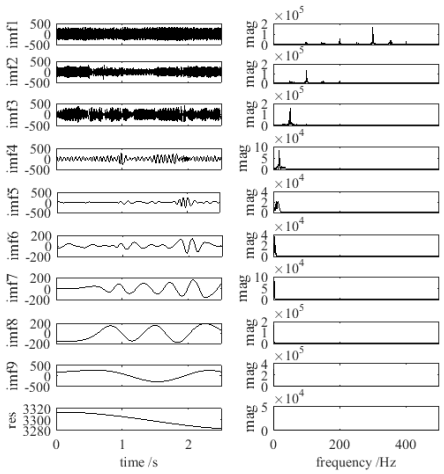

(b) IMFs by the EMD

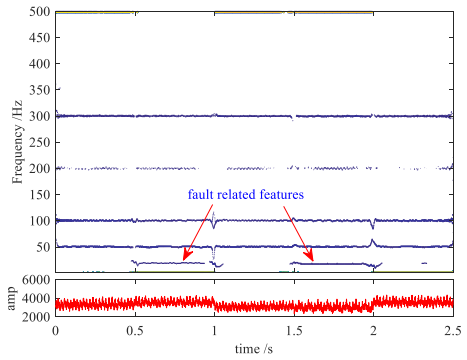

(c) Time-frequency map by the VMD

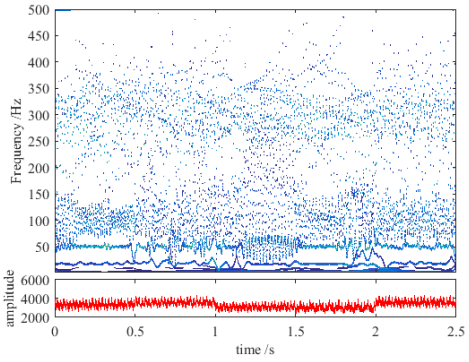

(d) Time-frequency map by the EMD

Fig.10 Detection of an electrical fault occurring in a 'WT' generator

5. Conclusions

In order to explore a more effective signal processing method for realizing reliable WT CM, the superiorities of the recently developed VMD over the EMD in noise robustness, tone detection, tone separation and instantaneous time-frequency feature extraction are investigated in this paper. From the work reported above, the following conclusions are reached:

- Attributed to the use of a bandwidth constrain condition depicted by (4) and (5), the VMD resultant modes have limited frequency bandwidth. By contrast, as the EMD does not perform any bandwidth checking in calculation, the obtained IMFs are not necessary narrow-band functions;
- The narrow-band modes obtained from the VMD are 'not exactly' but almost mono-component signals, of which the instantaneous time-frequency features can be accurately extracted with the aid of Hilbert transform. By contrast, the IMFs derived from the EMD

are not necessarily narrow-band functions, of which the instantaneous features cannot be correctly extracted by performing the Hilbert transform. Thus, the instantaneous time-frequency features of the signal being inspected are more likely to be successfully extracted by the VMD rather than by the EMD;

- The VMD outperforms the EMD also in intra-wave signal analysis because the EMD generates unidentified ripples at low frequencies, which spoil the time-frequency map thus make signal interpretation more difficult;
- In contrast to the EMD, the VMD is not only robust in against noise, but also efficient in detecting weak side-band features contained in the signal. These merits make the VMD ideal for processing real WT CM signals, which are often polluted by background noise and the fault induced features are usually weak and difficult to detect.

The experimental results depicted in Section 3 and WT CM results reported in Section 4 have provided convincing proofs to support the above conclusions although further verification is still required in the future. In view of these merits, to further improve the accuracy of the VMD by optimizing its parameters K and α and then turn the VMD to be a feasible in-situ WT CM technique will be a future work.

Acknowledgement

The work reported in the paper was supported by the Research Project of State Key Laboratory of Mechanical System and Vibration MSV201504 and Chinese Natural Science Foundation with the reference number of 11472103.

References

[1] Zaggout M., Tavner P., Crabtree C., Ran L.: 'Detection of rotor electrical asymmetry in wind turbine doubly-fed induction generators', IET Renewable Power Generation, 2014, **8**, (8), pp.878-886.

[2] Tavner P., D. Zappal, S. Sheng: 'Side-band algorithm for automatic wind turbine gearbox fault detection and diagnosis', IET Renewable Power Generation, 2014, **8**, (4), pp.380-389.

[3] Yang W., Little C., Tavner P., Court R.: 'Data-driven technique for interpreting wind turbine condition monitoring signals', IET Renewable Power Generation, 2014, **8**, (2), pp.151-159.

[4] Barton J.P., Watson S. J.: 'Analysis of electrical power data for condition monitoring of a small wind turbine', IET Renewable Power Generation, 2013, **7**, (4), pp.341-349.

[5] Wang Y., Infield D.: 'Supervisory control and data acquisition data-based non-linear state estimation technique for wind turbine gearbox condition monitoring', IET Renewable Power Generation, 2013, **7**, (4), pp.350-358.

[6] Yang W., Tavner P., Crabtree C., Feng Y., Qiu Y.: 'Wind turbine condition monitoring: technical and commercial challenges', Wind Energy, 2014, **17**, (5), pp.673-693.

[7] Feng Y., Qiu Y., Crabtree C., Long H., Tavner P.: 'Monitoring wind turbine gearboxes', Wind Energy, 2013, **16**, (5), pp.728-740.

[8] Peng Z., Tse P.W., Chu F.L.: 'A comparison of improved Hilbert-Huang transform and wavelet transform: Application to fault diagnosis for rolling bearing', Mechanical Systems and Signal Processing, 2005, **19**, pp.974-988.

[9] Smith J.S.: 'The local mean decomposition and its application to EEG perception data', Journal of the Royal Society Interface, 2005, pp.443-454.

[10] Frei M.G., Osorio I.: 'Intrinsic time-scale decomposition: time-frequency-energy analysis and real-time filtering of non-stationary signals', Proceedings of the Royal Society A, 2007, 463, pp.321-342.

[11] Wang Y., He Z., Zi Y.: 'A demodulation method based on improved local mean decomposition and its application in rub-impact fault diagnosis', Measurement Science and Technology, 2009, 20, pp.1-10.

[12] Yang W., Little C., Tavner P., Court R.: 'Data-driven technique for interpreting wind turbine condition monitoring signals', IET Renewable Power Generation, 2014, 8(2), pp.151-159.

[13] Van M., Kang H.J., Shin K.S.: 'Rolling element bearing fault diagnosis based on non-local means de-noising and empirical mode decomposition', IET Science, Measurement & Technology, 2014, **8**, (6), pp.571-578.

[14] Hang J., Zhang J., Cheng M.: 'Fault diagnosis of wind turbine based on multi-sensors information fusion technology', IET Renewable Power Generation, 2014, **8**, (3), pp.289-298.

[15] Antonino-Daviu J.A., Riera-guasp M., Pons-LIinares J., Roger-FoIch J., Perez R.B., CharIton-Perez C.: 'Toward condition monitoring of damper windings in synchronous motors via EMD analysis', IEEE Transactions on Energy Conversion, 2012, **27**, (2), pp.432-439.

[16] Li R., He D.: 'Rotational machine health monitoring and fault detection using EMD-based acoustic emission feature quantification', IEEE Transactions on Instrumentation and Measurement, 2012, **61**, (4), pp.990-1001.

[17] Yang W., Court R., Tavner P., Crabtree C.: 'Bivariate empirical mode decomposition and its contribution to wind turbine condition monitoring', Journal of Sound and Vibration, 2011, **330**, (15), pp.3766-3782.

[18] Yang W., Tavner P.: 'Empirical mode decomposition, an adaptive approach for interpreting shaft vibration signals of large rotating machinery', Journal of Sound and Vibration, 2009, **321**, (3-5), pp.1144-1170.

[19] Yan R.Q., Gao R.X.: 'Hilbert-huang transform-based vibration signal analysis for machine health monitoring', IEEE Transactions on Instrumentation and Measurement, 2006, **55**, (6), pp.2320-2329.

[20] Wu Z., Huang N.E., Chen X.: 'The multi-dimensional ensemble empirical mode decomposition method', Advances in Adaptive Data Analysis, 2009, **1**(3), pp.339-372.

[21] Huang N.E., Zheng S., Long S.R., Wu M.C., Shih H.H., Zheng Q.A., Yen N.C., Tung C.C., Liu H.H.: 'The empirical mode decomposition and the Hilbert spectrum for nonlinear and non-stationary time series analysis', Proceedings of the Royal Society of London A, 1998, 454, pp.903-995.

[22] Yang W.: 'Interpretation of mechanical signals using an improved Hilbert-Huang transform', Mechanical Systems and Signal Processing, 2008, 22, pp.1061-1071.

[23] Dragomiretskiy K., Zosso D.: 'Variational mode decomposition', IEEE Transactions on Signal Processing, 2014, **62**, (3), pp.531-544.

[24] Lv Z., Tang B., Zhou Y., Zhou C.: 'A novel method for mechanical fault diagnosis based on variational mode decomposition and multikernel support vector machine', Shock and Vibration, 2016, In Press.

[25] Lahmiri S.: 'Comparing variational and empirical mode decomposition in forecasting day-ahead energy prices', IEEE Systems Journal, 2016, In Press.

[26] An X., Zeng H.: 'Pressure fluctuation signal analysis of a hydraulic turbine based on variational mode decomposition', Journal of Power and Energy, 2015, 229(8), pp.978-991.

[27] Mohanty S., Gupta K.K., Raju K.S.: 'Comparative study between VMD and EMD in bearing fault diagnosis', Proceedings of the 9th International Conference on Industrial and Information Systems (ICIIS), Gwalior, India, 2014.

[28] Yang W., Tavner P., Crabtree C., Wilkinson M.: 'Cost-effective condition monitoring for wind turbines', IEEE Transactions on Industrial Electronics, 2010, **57**, (1), pp.263-271.